

# Nuclear structure of $^{76}\text{Ge}$ from inelastic neutron scattering measurements and shell model calculations

S. Mukhopadhyay,<sup>1,2,\*</sup> B. P. Crider,<sup>1</sup> B. A. Brown,<sup>3,4</sup> S. F. Ashley,<sup>1,2</sup> A. Chakraborty,<sup>1,2,†</sup> A. Kumar,<sup>1,2</sup> M. T. McEllistrem,<sup>1</sup> E. E. Peters,<sup>2</sup> F. M. Prados-Estévez,<sup>1,2</sup> and S. W. Yates<sup>1,2</sup>

<sup>1</sup>Department of Physics and Astronomy, University of Kentucky, Lexington, Kentucky 40506-0055, USA

<sup>2</sup>Department of Chemistry, University of Kentucky, Lexington, Kentucky 40506-0055, USA

<sup>3</sup>National Superconducting Cyclotron Laboratory, Michigan State University, East Lansing, Michigan 48824, USA

<sup>4</sup>Department of Physics and Astronomy, Michigan State University, East Lansing, Michigan 48824, USA

(Received 25 September 2016; revised manuscript received 4 December 2016; published 25 January 2017)

The low-lying, low-spin levels of  $^{76}\text{Ge}$  were studied with the  $(n, n'\gamma)$  reaction. Gamma-ray excitation function measurements were performed at incident neutron energies from 1.6 to 3.7 MeV, and  $\gamma$ -ray angular distributions were measured at neutron energies of 3.0 and 3.5 MeV. From these measurements, level spins, level lifetimes,  $\gamma$ -ray intensities, and multipole mixing ratios were determined. No evidence for a number of previously placed levels was found. Below 3.3 MeV, many new levels were identified, and the level scheme was re-evaluated. The  $B(E2)$  values support low-lying band structure. The  $2^+$  mixed-symmetry state has been identified for the first time. A comparison of the level characteristics with large-scale shell model calculations yielded excellent agreement.

DOI: [10.1103/PhysRevC.95.014327](https://doi.org/10.1103/PhysRevC.95.014327)

## I. INTRODUCTION

The nucleus  $^{76}\text{Ge}$  has taken on special significance as it decays by two-neutrino double- $\beta$  decay and is viewed as a favorable case for the observation of neutrinoless double- $\beta$  ( $0\nu\beta\beta$ ) decay [1]. If this rare  $0\nu\beta\beta$  decay process is observed, the mass of the neutrino could be obtained; however, this determination relies on nuclear structure calculations. One of the motivations for the present measurements was to provide data on the properties of low-lying states in  $^{76}\text{Ge}$  as input to these model calculations.

The nuclei in the Ge region exhibit many interesting structural features. The low-lying  $0^+$  states in the stable Ge nuclei have been interpreted as evidence for shape coexistence [2], which was established in  $^{72}\text{Ge}$  with multistep Coulomb excitation [3] and was recently extended to  $^{80}\text{Ge}$  [4]. Moreover, Toh *et al.* [5] proposed that  $^{76}\text{Ge}$  may be a rare example of a nucleus exhibiting rigid triaxial deformation in its low-lying states, i.e., that it follows the rigid triaxial rotor model of Davydov and Filipov [6] with a well-defined potential minimum at a nonzero value of  $\gamma$ . The defining feature on which this claim is based is the energy staggering in the  $\gamma$  band. Motivated by this experimental result, Nikšić and coworkers [7] performed calculations within the framework of nuclear density functional theory for the  $^{72-82}\text{Ge}$  isotopes. Their analysis did not confirm the interpretation for rigid triaxial deformation at low energy in  $^{76}\text{Ge}$ ; in fact, they arrived at the conclusion that the mean-field potential of  $^{76}\text{Ge}$  is  $\gamma$ -soft, more in keeping with the  $\gamma$ -unstable rotor model of Wilets and Jean [8].

In spite of many studies carried out in  $^{76}\text{Ge}$  with a number of different probes— $^{76}\text{Ga}$   $\beta^-$  decay [9], charged-particle scattering [10,11], neutron scattering [12], transfer reactions [13], and Coulomb excitation [14]—it is surprising that the low-lying levels of this nucleus are not better characterized. However, the recent detailed in-beam  $\gamma$ -ray spectroscopic investigation with the Gammasphere array by Toh *et al.* [5] contributed significantly to removing ambiguities in the literature and to establishing the ground,  $\gamma$ , and negative-parity bands in  $^{76}\text{Ge}$  to moderate spins. In the work presented here, we have focused on describing the structure of this nucleus through the measurement of lifetimes, branching ratios, and multipole mixing ratios combined with a careful construction of a detailed level scheme, ultimately leading to the determination of transition probabilities, and resolving questions about the nuclear structure in the low-energy and low-spin regime. With modern computer codes such as NUSHELLX [15] it is possible to carry out configuration interaction calculations in the  $\text{jj}44$  model space that includes the  $0f_{7/2}, 1p_{3/2}, 1p_{1/2}$ , and  $0g_{9/2}$  orbitals.

## II. EXPERIMENTAL DETAILS AND DATA ANALYSIS

The  $^{76}\text{Ge}(n, n'\gamma)$  experiments were performed at the University of Kentucky Accelerator Laboratory (UKAL) using methods described previously [16]. Protons from the 7-MV Van de Graaff accelerator were used to create nearly monoenergetic ( $\Delta E < 100$  keV) fast neutrons via the  $^3\text{H}(p, n)^3\text{He}$  reaction with a tritium gas target. The proton beam was pulsed at a 1.875-MHz rate with a pulse width of approximately 1 ns. The emitted neutrons then impinged upon a scattering sample, which consisted of 19.56 g of  $\text{GeO}_2$ , enriched to 84% in  $^{76}\text{Ge}$ , contained in a cylindrical polyethylene vial of 1.1-cm radius and 3.0-cm height. The primary contaminant in the sample arises from  $^{74}\text{Ge}$ , which was present at a level of 14% of the total composition.

\*smukh3@uky.edu

†Present address: Department of Physics, Siksha Bhavana, Visva-Bharati, Santiniketan 731235, India.

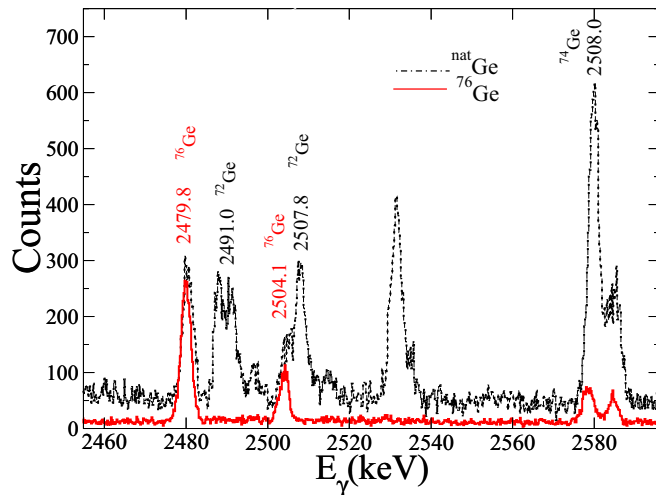


FIG. 1. Portion of the  $\gamma$ -ray spectrum from 3.5-MeV neutrons incident on the enriched  $^{76}\text{GeO}_2$  scattering sample (solid) and a comparison with  $^{\text{nat}}\text{Ge}$  (dashed) as the sample. The  $^{\text{nat}}\text{Ge}$  has been normalized to the  $^{76}\text{Ge}$  spectrum with respect to time and amount of  $^{76}\text{Ge}$  present. The peaks belonging to  $^{76}\text{Ge}$  have similar counts in both spectra.

Gamma-ray spectra were detected with a high-purity germanium (HPGe) detector of 50% relative efficiency and an energy resolution of 2.2 keV (FWHM) at 1333 keV surrounded by a bismuth germanate (BGO) annulus, which served as a Compton suppressor and active shield. Time-of-flight gating on the prompt gamma peak reduced the background from neutron interactions in the shielding, the HPGe detector, and surrounding materials.

A portion of the in-beam  $\gamma$ -ray spectrum obtained from the HPGe detector, located at  $90^\circ$  with respect to the beam axis at an incident neutron energy of 3.5 MeV, is shown in Fig. 1. In order to rule out  $\gamma$  rays arising from other Ge isotopes, particularly  $^{74}\text{Ge}$ , we measured spectra with neutrons on elemental Ge of natural abundance. A comparison of the spectra is shown in Fig. 1, where for example, the 2479.8-keV peak for the enriched  $^{76}\text{GeO}_2$  sample has similar counts as in the spectrum for normalized  $^{\text{nat}}\text{Ge}$ . This observation confirms that these  $\gamma$  rays arise from transitions between levels in  $^{76}\text{Ge}$ . The inelastic neutron scattering (INS) reaction non-selectively populates low-spin states up to the energy of the incident neutrons. This property was utilized to eliminate levels misplaced in previous studies.

### A. Excitation functions

Gamma-ray excitation functions were measured with a single HPGe detector at incident neutron energies between 1.6 and 3.7 MeV in steps of 100 keV at an angle  $90^\circ$  relative to the beam axis. A  $^{226}\text{Ra}$  source was used to calibrate the efficiency and determine the energy nonlinearity of the detector and data acquisition system. In addition, a long counter [17, 18] and a forward monitor were used to determine the relative neutron fluences when normalizing spectra at different neutron energies. The long counter is positioned at

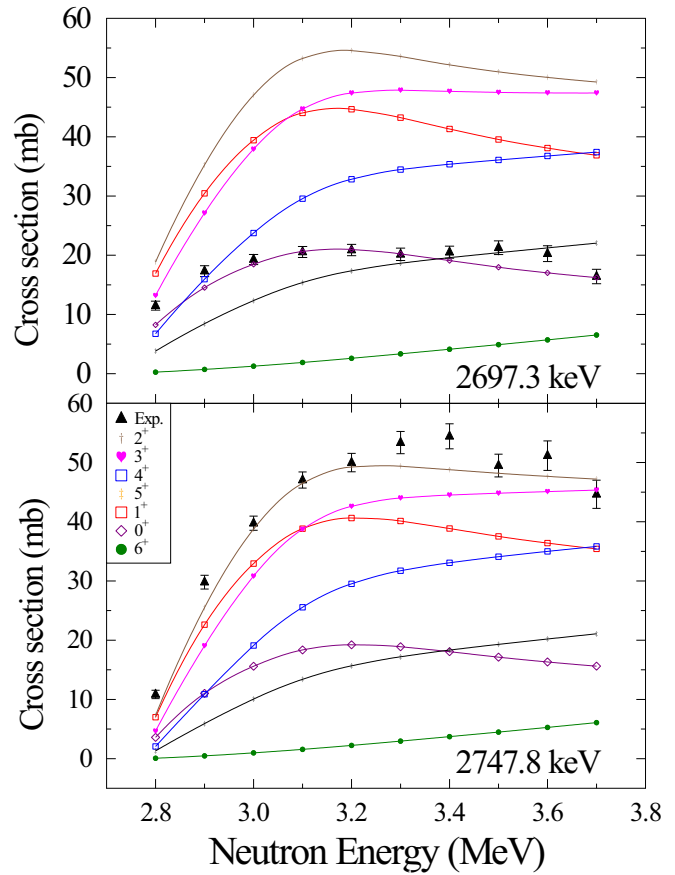


FIG. 2. Comparison of the excitation functions for the 2697.3-keV  $0^+$  and 2747.8-keV  $2^+$  levels with the theoretical cross sections calculated with the code CINDY [20].

$85^\circ$  with respect to the beam direction. At this angle, the source neutron energy is in a relatively smoothly varying region of the long counter efficiency curve [19] avoiding resonances. The forward monitor, an NE-213 scintillator, is placed at  $45^\circ$  and above the scattering plane to provide a direct, collimated view of the gas cell. Source neutrons are identified by time of flight with pulse-shape discrimination, the combination of which provides a very clean monitor of on-pulse neutron production. The accurate determination of the yield threshold for a particular  $\gamma$  ray was used to place uniquely the level from which the  $\gamma$  ray arises.

The energy thresholds for the  $\gamma$  rays were obtained from the excitation function plots. In addition, the relative experimental level cross sections can be compared with the theoretical cross sections computed by the statistical model code CINDY [20] to infer the spins of the levels. As examples, the excitation functions from the 2697.3- and 2747.8-keV levels, which have been assigned spins of  $0^+$  and  $2^+$ , respectively, are shown in Fig. 2.

### B. Angular distributions

Angular distributions of  $\gamma$  rays were measured at incident neutron energies of 3.0 and 3.5 MeV, where the emitted  $\gamma$  rays were detected at eleven angles from  $40^\circ$  to  $150^\circ$

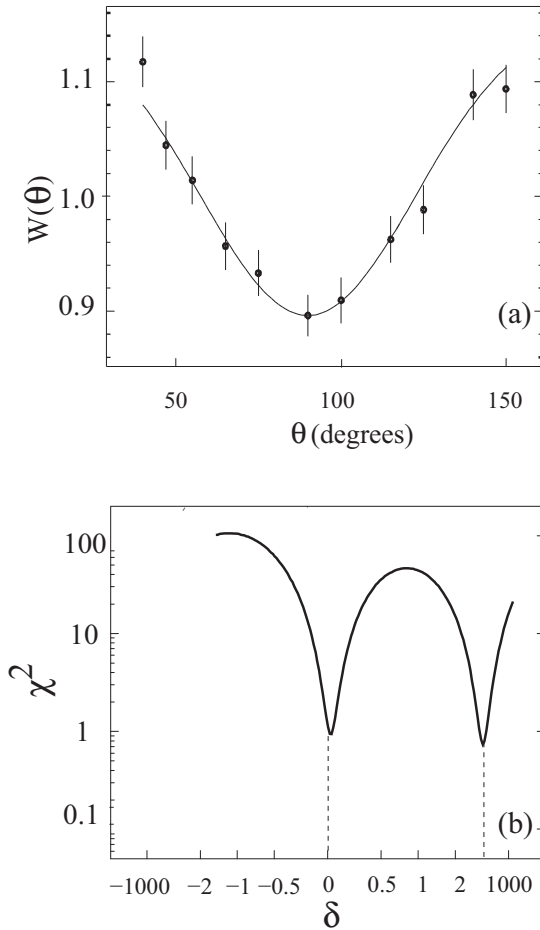


FIG. 3. (a) Angular distribution of the 2203.7-keV  $\gamma$  ray from the 2766.7-keV  $2^+$  state to the first excited state. (b)  $\chi^2$  vs  $\delta$  plot for the 2203.7-keV  $\gamma$  ray.

relative to the beam axis. At low incident neutron energies, the inelastic neutron scattering reaction occurs predominantly through compound nucleus formation. As this reaction leads to an alignment of the excited nuclei, the angular distributions of  $\gamma$  rays from the decays of the excited levels exhibit anisotropies reflecting this alignment, the spins of the levels, and the multiplicities of the transitions. The variation of the yield of a particular  $\gamma$  ray can be fit with a least-squares Legendre polynomial expansion, in which only the even-order terms contribute. This is given by

$$W(\theta) = A_0[1 + a_2 P_2(\cos \theta) + a_4 P_4(\cos \theta)], \quad (1)$$

where the angular distribution coefficients  $a_2$  and  $a_4$  depend on the level spins, multiplicities, and mixing ratios ( $\delta$ ), and  $A_0$  corresponds to the relative cross section of the  $\gamma$  ray. By fitting the angular distribution with Eq. (1) and comparing with calculations from the statistical model code CINDY [20],  $\delta$  values and level spins were determined. The angular distribution for the 2203.7-keV  $\gamma$  ray from the 2766.7-keV  $2_5^+$  level to the 562.9-keV  $2_1^+$  state is shown in Fig. 3.

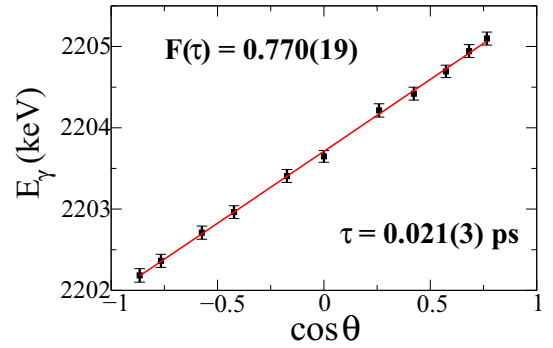


FIG. 4. Doppler-shift attenuation data for the 2203.7-keV  $\gamma$  ray from the 2766.7-keV level.

### C. Level lifetimes

Lifetimes of the excited levels were measured through the Doppler-shift attenuation method following the  $(n, n'\gamma)$  reaction [21]. The shifted  $\gamma$ -ray energy is given by

$$E_\gamma(\theta) = E_{\gamma_0} \left[ 1 + \frac{v_0}{c} F(\tau) \cos \theta \right] \quad (2)$$

with  $E_{\gamma_0}$  being the unshifted  $\gamma$ -ray energy,  $v_0$  the initial recoil velocity of the center of mass,  $\theta$  the angle of observation, and  $F(\tau)$  the experimental attenuation factor, which is related to the stopping process. Finally, the level lifetimes can be determined by comparison of the experimental  $F(\tau)$  values with those calculated using the Winterbon formalism [22]. An example of the Doppler shift of the 2203.7-keV  $\gamma$  ray from the new 2766.7-keV level is shown in Fig. 4.

## III. EXPERIMENTAL RESULTS

The spectroscopic information obtained from the present  $(n, n'\gamma)$  measurements is summarized in Table I. Many levels below 3.3 MeV reported in the Nuclear Data Sheets (NDS) compilation [23] should have been observed in the present work, but were not seen. As a comprehensive picture of the low-lying states in  $^{76}\text{Ge}$  is sought, we briefly discuss the levels whose existence is refuted. In addition, we make note of the experimental spectroscopic features for some states which differ from those reported previously. For the levels up to 2.841 MeV, the reported angular distribution data are from the measurements with 3.0-MeV neutrons, while those for higher-energy levels from the measurements with 3.5-MeV neutrons.

### A. Previously reported levels not observed in the current study

As a comprehensive picture of the nuclear level structure of  $^{76}\text{Ge}$  is sought for comparison with theoretical calculations, it is important to accept or exclude levels which have been placed in other studies [23]. The  $(n, n'\gamma)$  reaction is known to populate levels statistically at the incident neutron energies utilized in this study, and we expect to populate all of the low-lying, low-spin levels. Our criteria for refuting a previous level placement is that the level, with its assigned spin, should

TABLE I. Levels of  $^{76}\text{Ge}$  from the current ( $n, n'\gamma$ ) measurements. Transition probabilities are calculated for those levels whose lifetimes have been measured. Spins of the states ( $J_i^\pi$ ), level energies ( $E_i$ ),  $\gamma$ -ray energies ( $E_\gamma$ ), experimental attenuation factors [ $F(\tau)$ ], level lifetimes ( $\tau$ ), branching ratios (BR), multipole mixing ratios ( $\delta_\pm^+$  or  $\pi L$ ),  $B(E2) \downarrow$ , and  $B(M1) \downarrow$  values are listed. The  $\delta$  value with the lower  $\chi^2$  is used. Positive uncertainties are reported in the superscripts and the negative uncertainties in the subscripts. Newly assigned  $E_\gamma$ ,  $\tau$  and  $\delta$  from the present measurements are in *italics*, with new levels in **bold font**.

$E_i$ [keV]	$E_f$ [keV]	$J_i^\pi \rightarrow J_f^\pi$	$E_\gamma$ [keV]	$F(\tau)$	$\tau$ [ps]	BR (%)	$\delta_\pm^+$ or $\pi L$	$B(E2) \downarrow$ [W.u.]	$B(M1) \downarrow$ [ $\mu_N^2$ ]
562.90(7)	0	$2_1^+ \rightarrow 0_1^+$	562.93(3)		26.3(3) <sup>a</sup>	100	$E2$	29(1) <sup>a</sup>	
1108.44(6)	562.9	$2_2^+ \rightarrow 2_1^+$	545.51(5)		11.5(2) <sup>a</sup>	59.5(18)	+2.5(2)	39 <sub>4</sub> <sup>5a</sup>	0.003 <sub>0.003</sub> <sup>0.002a</sup>
	0	$2_2^+ \rightarrow 0_1^+$	1108.38(7)			40.5(18)	$E2$	0.90(3) <sup>a</sup>	
1409.96(8)	562.9	$4_1^+ \rightarrow 2_1^+$	847.06(5)		2.6(6) <sup>a</sup>	100	$E2$	38(9) <sup>a</sup>	
1539.36(7)	1108.4	$3_1^+ \rightarrow 2_2^+$	430.95(5)			41.9(30)	+0.84(4)		
	562.9	$3_1^+ \rightarrow 2_1^+$	976.44(6)			58.1(23)	+1.87 <sub>0.11</sub> <sup>0.17</sup>		
							+2.72(20)		
1911.11(12)	562.9	$0_2^+ \rightarrow 2_1^+$	1348.20(6)	0.035(12)	1.8 <sub>0.5</sub> <sup>0.9</sup>	100	$E2$	5(2)	
2021.70(8)	1539.4	$4_2^+ \rightarrow 3_1^+$	482.33(5)	0.030(12)	2.1 <sub>0.6</sub> <sup>1.5</sup>	7.8(8)	+0.48 <sub>0.07</sub> <sup>0.09</sup>	12 <sub>5</sub> <sup>6</sup>	0.02(1)
							+2.9(1)	56 <sub>32</sub> <sup>57</sup>	0.002(1)
	1410.0	$4_2^+ \rightarrow 4_1^+$	611.72(4)			37.1(16)	+0.29 <sub>0.09</sub> <sup>0.42</sup>	7 <sub>3</sub> <sup>4</sup>	0.04(2)
							+0.59 <sub>0.41</sub> <sup>0.14</sup>	23(13)	0.03 <sub>0.02</sub> <sup>0.03</sup>
	1108.4	$4_2^+ \rightarrow 2_2^+$	913.24(7)			55.1(22)	$E2$	18(8)	
2453.72(13)	1410.0	$6_1^+ \rightarrow 4_1^+$	1043.75(5)	0.141(70)	0.38 <sub>0.14</sub> <sup>0.42</sup>	100	$E2$	91 <sub>48</sub> <sup>55</sup>	
2487.08(10)	2021.7	$5_1^+ \rightarrow 4_2^+$	465.31(10)	0.039(13)	1.5 <sub>0.4</sub> <sup>0.8</sup>	9.8(9)	+0.65 <sub>0.18</sub> <sup>0.93</sup>	37 <sub>16</sub> <sup>42</sup>	0.03 <sub>0.02</sub> <sup>0.01</sup>
							+1.4(1.0)	85 <sub>67</sub> <sup>104</sup>	0.01 <sub>0.01</sub> <sup>0.02</sup>
	1539.4	$5_1^+ \rightarrow 3_1^+$	947.77(17)			90.2(30)	$E2$	33 <sub>11</sub> <sup>12</sup>	
2504.12(8)	1539.4	$2_3^+ \rightarrow 3_1^+$	964.68(5)	0.035(10)	1.7 <sub>0.4</sub> <sup>0.7</sup>	9.3(8)	+2.8 <sub>0.8</sub> <sup>1.1</sup>	3 <sub>2</sub> <sup>1</sup>	0.0004(3)
							+0.57 <sub>0.12</sub> <sup>0.18</sup>	0.7 <sub>0.2</sub> <sup>0.3</sup>	0.003(1)
	1410.0	$2_3^+ \rightarrow 4_1^+$	1094.22(12)			11.8(8)	$E2$	2(1)	
	1108.4	$2_3^+ \rightarrow 2_2^+$	1395.66(4)			58.3(30)	+1.9(2)	2(1)	0.002(1)
							+0.08(4)	0.02(1)	0.007(2)
	0	$2_3^+ \rightarrow 0_1^+$	2504.09(6)			20.6(10)	$E2$	0.05(2)	
2669.14(9)	2021.7	$4_3^+ \rightarrow 4_2^+$	647.44(4)	0.023(10)	2.8 <sub>0.8</sub> <sup>2.0b</sup>	14.2(7)	-0.01(10)	0.001(1)	0.009(4)
							+1.1(2)	10 <sub>5</sub> <sup>7</sup>	0.004 <sub>3</sub> <sup>2</sup>
	1539.4	$4_3^+ \rightarrow 3_1^+$	1129.80(10)			53.8(30)	+0.01(2)	0.001(1)	0.007(3)
	1410.0	$4_3^+ \rightarrow 4_1^+$	1259.12(5)			32.1(12)	-0.002(63)	0.00001(1)	0.003(1)
							+1.09(2)	0.78(40)	0.0020(2)
2692.34(8)	1410.0	$3_1^- \rightarrow 4_1^+$	1282.35(5)	0.210(14)	0.231(20)	10.7(7)	$E1$		
	1108.4	$3_1^- \rightarrow 2_2^+$	1583.93(3)			5.4(6)	$E1$		
	562.9	$3_1^- \rightarrow 2_1^+$	2129.34(6)			83.9(33)	$E1$		
<b>2697.26(9)</b>	1108.4	$0_3^+ \rightarrow 2_2^+$	1588.76(4)	0.056(18)	1.01 <sub>0.26</sub> <sup>0.52</sup>	21.1(10)	$E2$	0.9(3)	
	562.9	$0_3^+ \rightarrow 2_1^+$	2134.25(5)			78.9(31)	$E2$	0.8(3)	
2733.26(10)	1539.4	$4_4^+ \rightarrow 3_1^+$	1193.92(12)	0.100(15)	0.54 <sub>0.08</sub> <sup>0.10</sup>	26.9(11)	+4.3(9)	8 <sub>3</sub> <sup>4</sup>	0.001(4)
							+0.36 <sub>0.05</sub> <sup>0.06</sup>	1.0(2)	0.015(3)
	1108.4	$4_4^+ \rightarrow 2_2^+$	1624.78(5)			74.1(30)	$E2$	5(1)	
2747.75(8)	1539.4	$2_4^+ \rightarrow 3_1^+$	1208.35(8)	0.188(11)	0.262(30)	25.2(13)	+0.09(5)	0.14(1)	0.030(3)
	1108.4	$2_4^+ \rightarrow 2_2^+$	1639.30(5)			69.4(28)	-0.002(29)	0.00004(1)	0.03(3)
	562.9	$2_4^+ \rightarrow 2_1^+$	2184.83(6)			5.4(6)	+2.9 <sub>1.1</sub> <sup>3.3</sup>	0.16 <sub>0.07</sub> <sup>0.18</sup>	0.0001(1)
							-0.07 <sub>0.06</sub> <sup>0.15</sup>	0.0009(1)	0.001(1)
<b>2766.65(12)</b>	562.9	$2_5^+ \rightarrow 2_1^+$	2203.71(6)	0.770(19)	0.021(3)	97.4(40)	-0.09(2)	0.28(3)	0.24(3)
							+3.1(3) <sup>c</sup>	35 <sub>7</sub> <sup>9</sup>	0.02(1)
	0	$2_5^+ \rightarrow 0_1^+$	2766.65(8)			2.6(8)	$E2$	0.33(6)	

TABLE I. (Continued).

$E_i$ [keV]	$E_f$ [keV]	$J_i^\pi \rightarrow J_f^\pi$	$E_\gamma$ [keV]	$\overline{F}(\tau)$	$\tau$ [ps]	BR (%)	$\delta_-^+$ or $\pi L$	$B(E2) \downarrow$ [W.u.]	$B(M1) \downarrow$ [ $\mu_N^2$ ]
2841.64(13)	1108.4	$2_6^+ \rightarrow 2_2^+$	1733.06(14)	0.623(22)	0.040(4)	70.2 (30)	$+0.01_{0.02}^{0.03}$ $+2.3(3)^c$	0.00007(1) $40_9^{10}$	0.19(2) 0.03(1)
	562.9	$2_6^+ \rightarrow 2_1^+$	2278.84(14)			29.8(15)	$+3.0_{0.5}^{0.9}$ $-0.08(6)$	0.038(4) 5(1)	0.036(4) 0.004(1)
<b>2856.65(12)</b>	1410.0	$4_5^+ \rightarrow 4_1^+$	1446.79(9)	0.326(20)	0.140(12)	100	$-0.08(8)$	0.32(3)	0.13(1)
2897.51(12)	1108.4	$0_4^+ \rightarrow 2_2^+$	1789.23(13)	0.127(18)	$0.447_{0.063}^{0.081}$	27.6(14)	$E2$	1.4(3)	
	562.9	$0_4^+ \rightarrow 2_1^+$	2334.51(11)			72.4(30)	$E2$	1.0(2)	
2919.65(12)	1108.4	$I_7^+ \rightarrow 2_2^+$	1811.47(17)	0.125(15)	$0.219(20)$	12.5(7)	$-0.8_{0.6}^{6.3}$	$0.43_{0.2}^{2.0}$	$0.003_{0.013}^{0.002}$
	562.9	$I_7^+ \rightarrow 2_1^+$	2356.57(23)			19.1(10)	$+1.3_{0.9}^{5.0}$	$0.3_{0.2}^{1.2}$	$0.0013_{0.0041}^{0.0009}$
	0	$I_7^+ \rightarrow 0_1^+$	2919.53(17)			68.4(33)	$M1$		0.007(1)
2957.82(12)	2692.3	$5_1^- \rightarrow 3_1^-$	265.3(5)			3.5(6)	$E2$		
	1410.0	$5_1^- \rightarrow 4_1^+$	1547.95(15)			96.5(38)	$E1$		
<b>2985.99(8)</b>	1410.0	$(2,3)^+ \rightarrow 4_1^+$	1576.02(8)	0.318(14)	0.144(9)	18.8(11)			
	1108.4	$(2,3)^+ \rightarrow 2_1^+$	1877.76(12)			81.2(31)			
2993.81(8)	2021.7	$4_6^+ \rightarrow 4_2^+$	972.30(6)	0.08(19)	$0.72_{0.12}^{0.18}$	42.7(17)	$-0.61_{0.05}^{0.07}$	0.10(2)	0.035(9)
	1539.4	$4_6^+ \rightarrow 3_1^+$	1454.37(9)			7.8(8)	$-5.2_{3.6}^{7.5}$ $-0.08_{0.59}^{0.13}$	$0.7_{0.7}^{1.7}$ $0.004(2)$	0.0001(1) 0.002(1)
	562.9	$4_6^+ \rightarrow 2_1^+$	2430.91(5)			49.5(24)	$E2$	0.34(8)	
<b>3004.71(11)</b>	562.9	$0_3^+ \rightarrow 2_1^+$	2441.77(7)	0.173(22)	$0.309_{0.041}^{0.055}$	100	$E2$	1.58(24)	
3007.13(10) <sup>d</sup>	1108.4	$I_2^+ \rightarrow 2_2^+$	1898.73(6)	0.822(16)	0.017(2)	63.4(25)	$-0.8_{0.7}^{1.8}$	$23_{12}^{35}$	$0.20_{0.20}^{0.13}$
	0	$I_2^+ \rightarrow 0_1^+$	3007.07(8)			36.6(18)	$M1$		0.04(1)
<b>3021.07(12)</b>	1539.4	$(2,3)^+ \rightarrow 3_1^+$	1481.73(9)	0.115(12)	$0.490_{0.052}^{0.068}$	36.8(18)			
	1410.0	$(2,3)^+ \rightarrow 4_1^+$	1611.36(16)			15.9(9)			
	1108.4	$(2,3)^+ \rightarrow 2_2^+$	1912.59(13)			47.4(1.9)			
<b>3042.92(11)</b>	562.9	$(1,2,3)^+ \rightarrow 2_1^+$	2479.80(12)	0.426(18)	0.092(6)	100			
3052.47(12)	1539.4	$(3)^+ \rightarrow 3_1^+$	1513.15(9)	0.580(12)	0.052(7)	100	$-0.05_{0.05}^{0.06}$ $+1.64(2)$	0.28(1) $76_{13}^{15}$	0.31(1) 0.09(2)
<b>3062.00(11)</b>	1410.0	$(4,5)^+ \rightarrow 4_1^+$	1652.13(8)	0.271(33)	0.176(31)	100			
<b>3066.78(12)</b>	1539.4	$(2,3,4)^+ \rightarrow 3_1^+$	1527.46(9)	0.047(17)	$1.3_{0.4}^{0.8}$	100			
<b>3070.28(12)</b>	1410.0	$4_7^+ \rightarrow 4_1^+$	1660.41(10)	0.054(21)	$1.1_{0.3}^{0.7}$	100	$-0.13(8)$ $+1.5(3)$	0.05(2) $2.1_{1.2}^{5.0}$	$0.011_{0.0045}^{0.0005}$ $0.004_{0.002}^{0.001}$
<b>3091.93(14)</b>	1410.0	$(3,5)^+ \rightarrow 4_1^+$	1682.10(9)	0.141(17)	$0.386_{0.046}^{0.060}$	100			
<b>3129.85(8)</b>	1108.4	$2_7^+ \rightarrow 2_2^+$	2021.48(10)	0.152(13)	$0.354_{0.034}^{0.038}$	84.9(35)	$-0.31_{0.06}^{0.05}$ $+10_3^{11}$	0.27(4) $3_1^5$	0.015(2) 0.0002(1)
	0	$2_7^+ \rightarrow 0_1^+$	3129.78(8)			15.1(9)	$E2$	0.06(2)	
3141.28(10) <sup>d</sup>	562.9	$I_3^+ \rightarrow 2_1^+$	2578.40(8) <sup>e</sup>	0.496(15)	0.070(4)	38.9(11)	$+0.7_1^{15}$ $+3_3^{13}$	$0.76_{0.3}^{6.7}$ $1.6_{2.1}^{8.6}$	$0.01_{0.01}^{0.13}$ $0.002_{0.002}^{0.01}$
	0	$I_3^+ \rightarrow 0_1^+$	3141.17(7)			61.1(11)	$M1$		0.016(1)
3147.28(13) <sup>d</sup>	1539.4	$(2,3)^+ \rightarrow 3_1^+$	1608.29(13)	0.285(15)	$0.164_{0.011}^{0.013}$	63.3(13)			
	1108.4	$(2,3)^+ \rightarrow 2_2^+$	2038.89(15)			8.4(10)			
	562.9	$(2,3)^+ \rightarrow 2_1^+$	2584.34(10)			28.3(12)			
<b>3162.52(12)</b>	1410.0	$(4)^+ \rightarrow 4_1^+$	1752.65(5)	0.778(19)	0.021(3)	100	$-0.09(9)$ $+1.4(3)$	1.0(1) $80_{20}^{25}$	0.50(5) $0.18_{0.05}^{0.06}$
3181.92(11)	2692.3	$(2,3)^+ \rightarrow 3_1^-$	489.73(9)	0.068(27)	$0.85_{0.26}^{0.60}$	25.1(19)			
	562.9	$(2,3)^+ \rightarrow 2_1^+$	2618.93(6)			74.9(37)			

TABLE I. (*Continued*).

$E_i$ [keV]	$E_f$ [keV]	$J_i^\pi \rightarrow J_f^\pi$	$E_\gamma$ [keV]	$\overline{F}(\tau)$	$\tau$ [ps]	BR (%)	$\delta_\pm^+$ or $\pi L$	$B(E2) \downarrow$ [W.u.]	$B(M1) \downarrow$ [ $\mu_N^2$ ]
<b>3190.98(8)</b>	1108.4	$2^+ \rightarrow 2_2^+$	2082.51(9)	0.258(19)	0.185(20)	23.1(17)	$-3_3^{13}$	$1.2_{1.4}^{6.7}$	$0.000_{0.0027}^{0.0008}$
	562.9	$2^+ \rightarrow 2_1^+$	2628.08(12)			67.6(27)	$-1_1^{20}$ $+0.36_{0.10}^{0.21}$	$0.6_{0.2}^{8.8}$ $0.14(3)$	$0.005_{0.059}^{0.002}$ $0.010(2)$
	0	$2^+ \rightarrow 0_1^+$	3190.99(4)			9.3(9)	$+1.03_{0.81}^{0.25}$ $E2$	$0.75_{0.44}^{0.22}$ $0.06_{0.02}^{0.03}$	$0.005_{0.001}^{0.003}$
<b>3199.81(13)</b>	1108.4	$(3)^+ \rightarrow 2_2^+$	2091.67(14)	0.059(40)	$1.0_{0.4}^{2.3}$	44.9(23)	$+0.05_{0.01}^{0.09}$ $-7_3^{14}$	$0.001(1)$ $0.5_{0.4}^{2.5}$	$0.003(2)$ $0.00005(9)$
	562.9	$(3)^+ \rightarrow 2_1^+$	2636.64(27)			55.1(22)	$-8_3^{13}$ $0.08(8)$	$0.18_{0.16}^{0.81}$ $0.001(1)$	$0.00002(4)$ $0.002_{0.012}^{0.014}$
	3235.94(13)	$(5)^+ \rightarrow 4_2^+$	1214.23(11)	0.616(26)	$0.044_{0.004}^{0.005}$	45.9(22)	$+2.2_{1.8}^{3.1}$	$40_{130}^{270}$	$0.05_{0.05}^{0.07}$
	1410.0	$(5)^+ \rightarrow 4_1^+$	1826.18(12)			54.1(22)	$+0.48_{0.20}^{0.13}$ $+1.9_{1.7}^{1.0}$	$5(1)$ $21_{10}^{15}$	$0.09(2)$ $0.02_{0.01}^{0.03}$
<b>3243.80(12)</b>	562.9	$1^+ \rightarrow 2_1^+$	2680.90(10)	0.539(20)	$0.059_{0.004}^{0.005}$	85.6(41)	$-4_2^{60}$ $+0.04(2)$	$4_3^{92}$ $0.006(1)$	$0.003_{0.500}^{0.002}$ $0.04(1)$
	0	$1^+ \rightarrow 0_1^+$	3243.66(9)			14.4(10)	$M1$		$0.004(1)$

<sup>a</sup>The lifetime used for calculating the reduced transition probabilities is taken from the Nuclear Data Sheets [23].

<sup>b</sup>The lifetime is from the 3.5-MeV angular distribution data.

<sup>c</sup>This value of  $\delta$  is reported as obtained from the angular distribution data. The  $B(E2)$  for this value is unrealistic; and therefore, we adopt the other value.

<sup>d</sup>Level and  $\gamma$ -ray energies differ from previous  $(n, n'\gamma)$  reaction results [28]. The level properties reported here are from measurements close to the level energy and, therefore, feeding arising from higher-lying levels could be avoided.

<sup>e</sup>The 2578.40-keV  $\gamma$  ray is not resolved from the 2580.07-keV  $\gamma$  ray from the  $3^-$  level at 3175.5 keV in  $^{74}\text{Ge}$ .

exhibit a significant cross section and that the previously suggested de-excitation  $\gamma$  rays are not observed. Previously reported levels which are refuted by the current data are discussed below.

- (i) *2019.9-keV* ( $4^+$ ) level: The 911.4-keV  $\gamma$  ray [9] was not observed in any spectra.
- (ii) *2204.9-keV* ( $1, 2^+$ ) level: Gamma rays of 1097.4 and 2203.8 keV were reported from this level [12]. In our work, the 2203.7-keV  $\gamma$  ray was reassigned to a level at 2766.7 keV (see the discussion of the  $2_5^+$  state). The 1097.4-keV  $\gamma$  ray has a very small cross section and could not be accommodated in the  $^{76}\text{Ge}$  level scheme.
- (iii) *2284.2-keV* ( $3^-$ ) level: The reported 1175.7-keV  $\gamma$  ray [9] is not present in our spectra.
- (iv) *2456.0-keV* level: We find no evidence for the level at 2456(5) keV observed only in  $^{76}\text{Ge}(p, p')$  measurements [10].
- (v) *2478.2-keV* ( $1, 2^+$ ) level: This level, placed previously from the  $(n, n'\gamma)$  reaction with reactor neutrons [12], is not included in the level scheme, as neither of the reported  $\gamma$  rays, 1915 and 2478.2 keV, are present in our spectra.
- (vi) *2554.0-keV* level: We find no evidence for the level at 2554(5) keV observed in  $^{76}\text{Ge}(p, p')$  measurements [10].
- (vii) *2591.1-keV* ( $1^+, 2^+$ ) level: The previously assigned 1051.7- and 2591.0-keV  $\gamma$  rays, which were ob-

served in the  $^{76}\text{Ga}$   $\beta^-$  decay [9] to establish this level, were not present in our spectra. We observe a 1481.7-keV  $\gamma$  ray, which is close in energy to the reported third branch from this level, but the threshold is 3.1 MeV. This  $\gamma$  ray is rather attributed to the 3021.1-keV level.

- (viii) *2624.0-keV* level: We find no evidence for the level at 2624(5) keV tentatively observed in  $^{76}\text{Ge}(p, p')$  measurements [10].
- (ix) *2654.5-keV* ( $\leq 4$ ) level: This level was observed in the  $^{76}\text{Ga}$   $\beta^-$  decay [9], with reported  $\gamma$  rays at 1546.0 and 2091.9 keV. We do not observe a 1546.0-keV  $\gamma$  ray and the 2091.3-keV  $\gamma$  ray has a threshold of 3.4 MeV.
- (x) *2768.8-keV*  $2^+$  level: The reported 1358.9-keV  $\gamma$  ray [9] was not observed in our spectra, and the 1660.40-keV  $\gamma$  ray has a threshold energy of 3.2 MeV and has been reassigned to the 3070.4-keV level.
- (xi) *2921.0-keV*  $3^-$  level: We find no evidence for the level at 2921(5) keV observed in the  $^{76}\text{Ge}(p, p')$  and  $^{76}\text{Ge}(\alpha, \alpha')$  reactions [10, 11].
- (xii) *2962.3-keV* ( $5^-$ ) level: No evidence for this level was found; however, as will be discussed later, a  $5^-$  state is placed at 2957.9 keV.
- (xiii) *2988.2-keV* level: This level with 319.0-, 500.9-, and 534.4-keV  $\gamma$  rays reported by Toh *et al.* [5] was not observed, but this may reflect its higher spin.

**B. New levels and levels with new spectroscopic information**

- (i) *1911.1-keV  $0_2^+$  level*: The lifetime for the  $0_2^+$  state was determined to be  $1.8_{-0.5}^{+0.9}$  ps with a  $B(E2; 0_2^+ \rightarrow 2_1^+)$  of 5(2) W.u. for the only observed decay.
- (ii) *2021.7-keV  $4_2^+$  level*: This level, suggested by Dostemesova *et al.* [12] as a ( $4^+$ ) state, with 482.3-, 611.7-, and 913.2-keV  $\gamma$  rays to the  $3_1^+$ ,  $4_1^+$ , and  $2_2^+$  states, respectively, has a lifetime of  $2.1_{-0.6}^{+1.5}$  ps. Both of the possible  $\delta$  values for the 482.3- and 611.7-keV transitions are reported in Table I. The value of  $\delta$  for the 611.7-keV transition is reported to be 0.50(8) in Ref. [5], which agrees well with our measured value of  $0.59_{-0.41}^{+0.14}$ .
- (iii) *2453.7-keV  $6_1^+$  level*: The decay of the  $6_1^+$  state was observed by Toh *et al.* [5]. The lifetime obtained in the present work,  $0.38_{-0.14}^{+0.42}$  ps, has a large uncertainty as this level has a relatively small inelastic neutron scattering cross section. The  $B(E2; 6^+ \rightarrow 4^+)$  of  $91_{-48}^{+55}$  W.u. is consistent with the collectivity expected for the lowest  $6^+$  excitation.
- (iv) *2487.1-keV  $5_1^+$  level*: This level was reported by Toh *et al.* [5] with branches to the  $4_2^+$  and  $3_1^+$  states. A 1077.2-keV  $\gamma$  ray to the  $4_1^+$  state was regarded as tentative [5], and is not observed in our work. The lifetime obtained for this level is  $1.5_{-0.4}^{+0.8}$  ps, and the intensities of the 465.3- and 947.8-keV  $\gamma$  rays are in good agreement with those in Ref. [5]. The  $B(E2; 5_1^+ \rightarrow 3_1^+)$  of  $33_{-11}^{+12}$  W.u. and  $B(E2; 5_1^+ \rightarrow 4_2^+)$  of  $37_{-16}^{+42}$  W.u. or  $85_{-67}^{+104}$  W.u. depending on the multipole mixing ratio chosen, confirm the collective nature of this level.
- (v) *2504.1-keV  $2_3^+$  level*: Dostemesova *et al.* [12] reported this level with 1395.1- and 2503.6-keV  $\gamma$  rays to the  $2_2^+$  and  $0_1^+$  states, respectively. Additional 964.7- and 1094.2-keV branches from this level to the  $3_1^+$  and  $4_1^+$  states have been identified in the present work. The measured lifetime for this level is  $1.7_{-0.4}^{+0.7}$  ps, which differs significantly from the previously reported value of  $0.35_{-0.15}^{+0.80}$  ps [12]. The  $B(E2)$  values for the transitions given in Table I indicate that this level is not collective.
- (vi) *2669.1-keV  $4_3^+$  level*: This level was placed by Toh *et al.* [5], but no spin was assigned. The transition intensities of the three decays agree well with those reported in Ref. [5]. The excitation function and the normalized cross section data support a spin assignment of  $4^+$  for this level, as does the angular distribution for the 1129.8-keV  $\gamma$  ray. We were able to obtain a level lifetime of  $2.8_{-0.8}^{+2.0}$  ps from the 3.5-MeV angular distribution data.
- (vii) *2692.3-keV  $3_1^-$  level*: This level was reported in the NDS [23] with branches to the  $4_1^+$ ,  $2_2^+$ ,  $2_1^+$ , and  $0_1^+$  states; however, we fail to observe the ground-state transition. A 2690.6-keV  $\gamma$  ray is observed in our spectra from the 2690.6-keV  $1^+$  level in  $^{74}\text{Ge}$ , which may have masked the weak 2691.6-keV  $\gamma$  ray in  $^{76}\text{Ge}$  reported in  $^{76}\text{Ga}$   $\beta^-$  decay only [9]. The lifetime obtained for this level from our measurement, 0.231(20) ps, differs somewhat from the reported value of  $0.40_{-0.12}^{+0.22}$  ps [12]. Reduced transition probabilities of  $B(E1; 3_1^- \rightarrow 4_2^+) = 0.12(1)$  mW.u.,  $B(E1; 3_1^- \rightarrow 2_2^+) = 0.03(1)$  mW.u., and  $B(E1; 3_1^- \rightarrow 4_1^+) = 0.20(2)$  mW.u. were determined.
- (viii) *2697.3-keV  $0_3^+$  level*: Observed here for the first time, this level decays to the  $2_2^+$  and  $2_1^+$  states via 1588.8- and 2134.3-keV  $\gamma$  rays, respectively. The isotropic angular distributions for both  $\gamma$  rays, along with the excitation function (see Fig. 2), leads us to assign a spin of  $0^+$ . The level lifetime obtained is  $1.01_{-0.26}^{+0.52}$  ps, and the  $B(E2)$  values of  $\leq 1$  W.u. indicate that this level is not collective.
- (ix) *2733.3-keV  $4_4^+$  level*: This level, with branches to the  $3_1^+$  and  $2_2^+$  states, was reported by Toh *et al.* [5], although the transition intensities for the 1193.9- and 1624.8-keV  $\gamma$  rays differ from our values. The 1624.8-keV  $\gamma$  ray was not reported by Dostemesova *et al.* [12]. The lifetime determined for this level is  $0.54_{0.08}^{0.10}$  ps, which also differs from the reported lifetime of  $0.25_{-0.12}^{+0.26}$  ps in Ref. [12]. Two possible values of the mixing ratios were obtained for the 1193.9-keV ( $4_4^+ \rightarrow 3_1^+$ ) transition (see Table I) and both provide similar  $\chi^2$  values.
- (x) *2747.8-keV  $2_4^+$  level*: The NDS gives possible spins between 1 and 4 for this level [23], but from our experimental results (see Fig. 2) a spin of  $2^+$  is assigned to this state. The measured lifetime is 0.262(30) ps which has a smaller uncertainty than the previously reported value of  $0.48_{-0.17}^{+0.48}$  ps [23]. This level decays to the  $3_1^+$ ,  $2_2^+$ , and  $2_1^+$  states with small  $B(E2)$  values.
- (xi) *2766.7  $2_5^+$  level*: This level will be discussed in Sec. VB.
- (xii) *2856.7-keV  $4_5^+$  level*: The 1446.8-keV  $\gamma$  ray, observed for the first time in this work, has a threshold energy of 3.1 MeV and decays to the  $4_1^+$  level at 1410.0 keV. The  $\delta$  value of  $-0.08(8)$  has the lower  $\chi^2$ , and the lifetime of this level is 0.140(12) ps. A relatively large  $B(M1) = 0.13(1) \mu_N^2$  is determined.
- (xiii) *2897.5-keV  $0_4^+$  level*: In addition to the decay branch to the  $2_1^+$  state reported in Ref. [12], a 1789.2-keV  $\gamma$  ray from this level to the  $2_2^+$  state has been placed. The lifetime for the state was found to be  $0.447_{-0.063}^{+0.081}$  ps.
- (xiv) *2919.7-keV  $1_1^+$  level*: In agreement with previous data [9,12], decay branches from this level to the  $2_2^+$ ,  $2_1^+$ , and  $0_1^+$  states were observed. Spins of 1 or  $2^+$  were suggested for this state [12,23]. The angular distribution of the 2919.5-keV ground-state transition,  $a_2 = -0.17(3)$  and  $a_4 = -0.08(5)$ , limits the spin of the state to  $J = 1$ . The measured lifetime is 0.219(20) ps and is consistent with the reported value of  $0.30_{-0.09}^{+0.14}$  ps [12].
- (xv) *2957.8-keV  $5_1^-$  level*: A  $5_1^-$  level at 2958.6 keV with a 1548.5-keV  $\gamma$  ray to the  $4_1^+$  state was reported by Toh

*et al.* [5]. We observed a 1548.0-keV  $\gamma$  ray, which is slightly different in energy but has the expected excitation energy threshold.

- (xvi) *2986.0-keV (2,3)<sup>+</sup> level*: Newly observed  $\gamma$  rays at 1576.0 and 1877.8 keV with a threshold energy of 3.1 MeV give rise to a new level at 2986.0 keV with a measured lifetime of 0.144(9) ps. The angular distribution of the 1877.8-keV  $\gamma$  ray restricts the spin to (2,3)<sup>+</sup>.
- (xvii) *2993.8-keV 4<sub>6</sub><sup>+</sup> level*: We observe three decay branches from this level—972.3 keV to the 4<sub>2</sub><sup>+</sup> state, 1454.4 keV to the 3<sub>1</sub><sup>+</sup> state, and 2430.9 keV to the 2<sub>1</sub><sup>+</sup> state—and the spin assignment is 4<sup>+</sup>. Previously, a 2994-keV level with spin 4<sup>+</sup> was observed in <sup>76</sup>Ge(*p*, *p'*) measurements [10]. A lifetime of 0.72<sub>0.12</sub><sup>0.18</sup> ps was measured for this level.

#### IV. SHELL MODEL CALCULATIONS

We have carried out configuration interaction (CI) calculations in the *jj44* model space (see Appendix), that consists of the  $0f_{7/2}, 1p_{3/2}, 1p_{1/2}$ , and  $0g_{9/2}$  orbitals for protons and neutrons using the shell-model code NUSHELLX [15]. The *M*-scheme dimension is about  $3.5 \times 10^6$ . We use two Hamiltonians that are appropriate for this model space, JUN45 [26] and *jj44b* [27]. Both of these have been widely used in connection with comparison to nuclear data in the mass region  $A = 60$ –100.

Both JUN45 and *jj44b* start with a realistic interaction based on the Bonn-C potential renormalized to the *jj44* model space with respect to a closed core for <sup>56</sup>Ni. Both have an assumed mass dependence of  $(A/58)^{-0.3}$ . The Hamiltonian is represented by 133 two-body matrix elements (TBME) and four single-particle energies (SPE). In both cases the single-valued decomposition method (SVD) was used to modify the *k* most well-determined linear combinations based on a least-squares fit to binding energies and excitation energies for a subset of the nuclei covered by the *jj44* model space. The remaining  $137 - k$  combinations of TBME and SPE were fixed at the initial Bonn-C starting values.

For the JUN45 Hamiltonian,  $k = 45$  linear combinations were determined by a fit to about 400 data points for 69 nuclei with  $N = 30$ –32 and  $Z = 46$ –50, as shown in Fig. 1 of Ref. [26] with an rms deviation of 185 keV. These data included the ground state and first three excited states in <sup>76</sup>Ge. For the *jj44b* Hamiltonian,  $k = 30$  linear combinations were determined from a fit to 550 data points for 77 nuclei with  $N = 48$ –50 and  $Z = 28$ –30 with an rms deviation of 240 keV. These data do not include <sup>76</sup>Ge.

The excitation energies are compared with experiment in Fig. 5. The experimental excitation energies are systematically about 200 keV lower than both JUN45 and *jj44b*.

$E2$  strengths for all possible transitions connecting the low-spin states of <sup>76</sup>Ge up to 4 MeV following the shell model calculations and experimental values up to 3 MeV are shown in Fig. 6. The isoscalar effective charge of  $e_p + e_n = 2.6$  was chosen to reproduce the experimental 2<sup>+</sup> to 0<sup>+</sup>  $B(E2)$  for the *jj44b* Hamiltonian. This is the same isoscalar effective charge derived from a fit to a wider set of data in Ref. [26]. The data

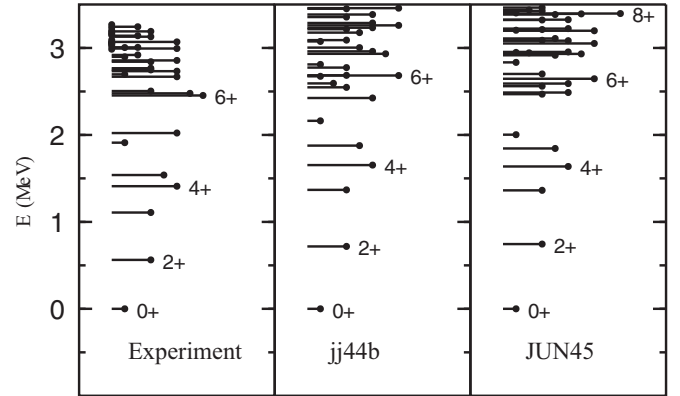


FIG. 5. Comparison of experimental and theoretical (shell model) level energies for the positive-parity states of <sup>76</sup>Ge. Levels with the same spin are indicated with lines of the same length.

are insensitive to the isovector effective charge and we use  $e_p - e_n = 1.0$ .

#### V. DISCUSSION

##### A. Band structure in <sup>76</sup>Ge

In above-barrier Coulomb excitation measurements by Toh *et al.* [5], band structures were identified in <sup>76</sup>Ge with ground-band and  $\gamma$ -band structures developed to moderate spin; however, these relationships were based only on branching

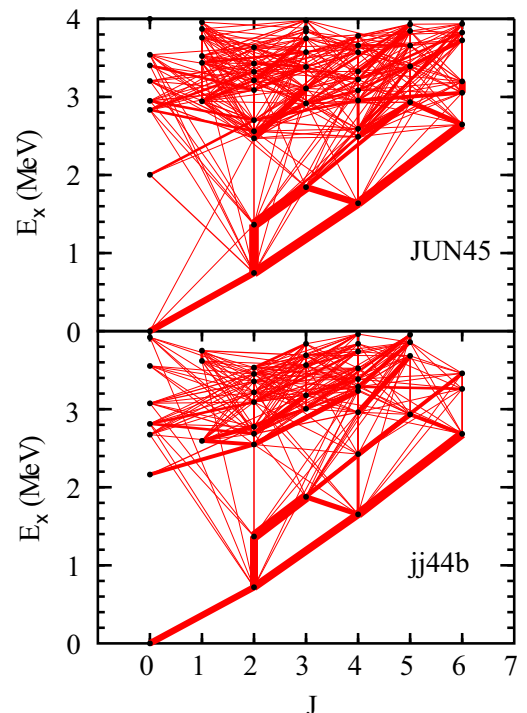


FIG. 6. Levels in <sup>76</sup>Ge connected by bars whose widths are proportional to the  $B(E2)$  values obtained with experiment and the shell model calculations. Only those transitions which decay with  $B(E2)$  values larger than one W.u. are depicted in the figure.



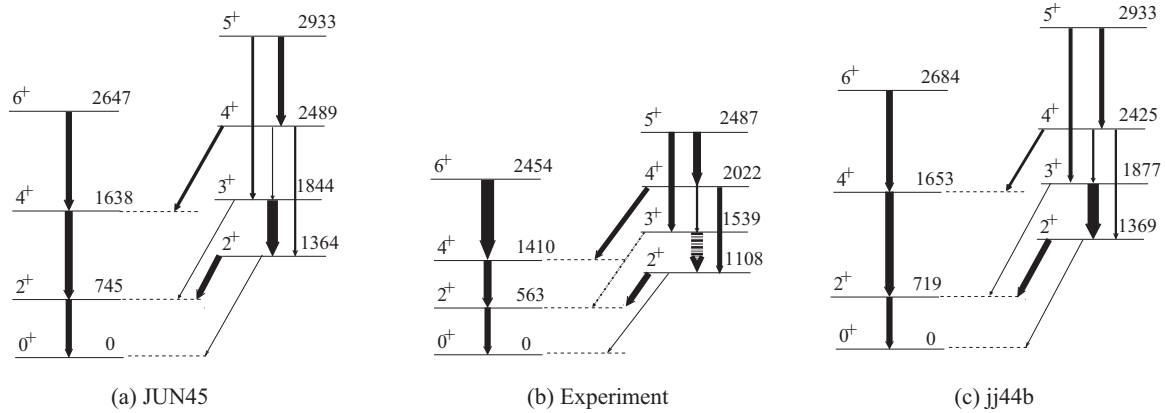


FIG. 7. Partial level scheme of  $^{76}\text{Ge}$  from shell model calculations [(a) and (c)] and experiment (b). The thicknesses of the solid arrows are proportional to the  $B(E2)$ s. Dashed arrows indicate that the level lifetime was not determined and the  $B(E2)$ s are calculated using the lifetime from shell-model calculations.

patterns and  $\gamma$ -ray intensities. Figure 7 shows the observed low-lying band structure. The  $E2$  transition rates measured here reinforce this picture. For example, the lowest  $5^+$  state, assigned as a member of the  $\gamma$  band, decays with large  $B(E2)$ s to the  $4_2^+$  and  $3_1^+$  states, which are interpreted as low-lying members of the band, and the decay to the lower-lying  $4_1^+$  state, an out-of-band transition, is not observed. Moreover, the theoretical and experimental  $B(E2)$  strengths for the ground-band and the  $\gamma$ -band transitions agree well. The excellent agreement with shell model calculations shows that the band structure can be produced from a microscopic basis.

### B. Mixed-symmetry state in $^{76}\text{Ge}$

The lowest  $2^+$  state has an isoscalar structure where collective proton and neutron components of the wave function are in phase. The mixed-symmetry state has similar collective proton and neutron components, but they are out of phase, giving rise to a strong isovector  $E2$  transition from the  $0^+$  ground state and a strong  $M1$  transition between the isoscalar and isovector collective states (since the  $M1$  operator is dominated by the isovector part). We can investigate the structure of the shell-model wave functions by calculating  $B(E2)_{IS}$  and  $B(E2)_{IV}$  from the ground state. These  $B(E2)$ s are defined in terms of their proton and neutron matrix elements,  $M_p$  and  $M_n$ , respectively [24]. The electromagnetic  $B(E2)$  is given by  $M_p^2/(2J+1)$ . The isoscalar combination is  $M_0 = (M_p + M_n)/2$  and the isovector combination is  $M_1 = (M_p - M_n)$ . In Fig. 8, we show the isoscalar  $B(E2)_{IS} = M_0^2$  and the isovector  $B(E2)_{IV} = M_1^2$  from the ground state to the lowest ten  $2^+$  states. As expected, the isoscalar  $E2$  is completely dominated by the first  $2^+$  state.

In a previous  $(n, n'\gamma)$  measurement [12], a 2204.9-keV level was reported with a 1097.4-keV  $\gamma$  ray to the  $2_1^+$  level and a 2203.8-keV branch to the ground state. With the threshold energy about 2.8 MeV for the 2203.7-keV  $\gamma$  ray in the excitation function measurement, we assign the 2203.7-keV  $\gamma$  ray to a new level at 2766.7 keV. From the Doppler-shift data shown in Fig. 4, a lifetime of  $\tau = 0.021(3)$  ps was determined for this level. [Note that the lifetime for the 2204.9-keV

level reported in Ref. [12] is 14(6) fs.] From the 3.0-MeV angular distribution measurement (see Fig. 3), we could extract the transition intensities and the multipole mixing ratios for transitions from this level. Experimental level cross sections for the 2203.67-keV  $\gamma$  ray were compared with the theoretical cross sections computed with the code CINDY [20] to infer a spin of  $2^+$  [see Fig. 3(b)].

In addition to the 2203.7-keV  $\gamma$  ray, we observe a 2766.6-keV  $\gamma$  ray in the 3.0-MeV angular distribution spectra. To obtain statistical improvement, we have summed the angular distribution spectra (without applying Doppler corrections to the individual spectra) as shown in Fig. 9, and hence we see a Doppler-broadened 2766.7-keV peak. The 2754.0-keV  $\gamma$  ray is from a  $^{24}\text{Na}$  radioactive source, which was used for online calibration. Table I contains the spectroscopic information obtained for the 2766.7-keV level.

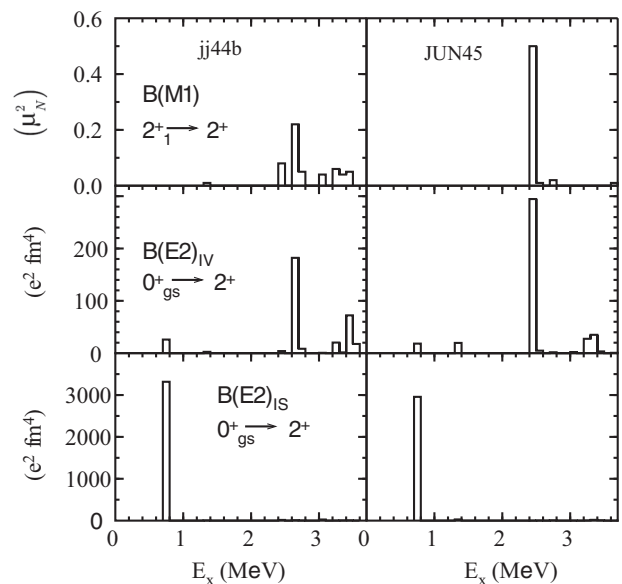


FIG. 8.  $B(M1)$ ,  $B(E2)_{IV}$ , and  $B(E2)_{IS}$  strength from shell-model calculations. See the text for more details.

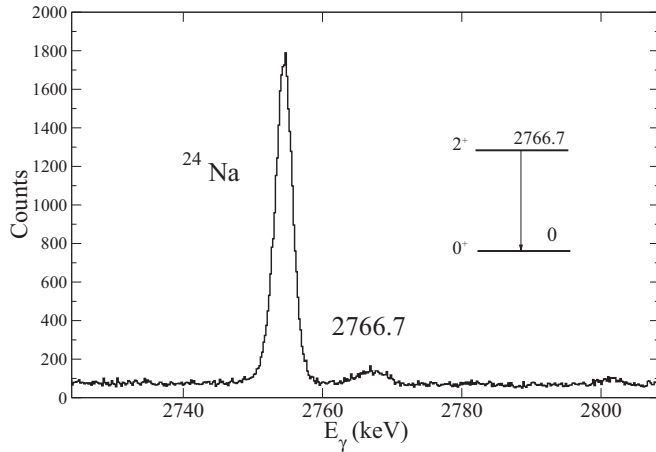


FIG. 9. Portion of the summed  $\gamma$ -ray spectrum. See the text for more details.

Figure 3 shows the angular distribution for the 2203.7-keV  $\gamma$  ray, and the fit to these data gives multipole mixing ratios of  $3.09_{-0.32}^{+0.35}$  and  $-0.09(2)$ . For the larger mixing ratio, the  $B(E2; 2_5^+ \rightarrow 2_1^+)$  would be  $36_{-7}^{+10}$  W.u., which is unusually large for a  $2^+$  state in this energy region. For the other value of  $\delta$ , these data give a large  $B(M1; 2_5^+ \rightarrow 2_1^+)$  value of  $0.24(3) \mu_N^2$ , which is of the order of magnitude expected for a mixed-symmetry state [25]. Accompanying this large  $B(M1)$  should be a small  $B(E2)$  to the ground state, and  $B(E2; 2_5^+ \rightarrow 0_1^+) = 0.33(6)$  W.u. is determined.

With the JUN45 Hamiltonian we see a very sharp isovector state at 2.47 MeV. Figure 8 also shows the  $B(M1)$  from the lowest  $2^+$  state to the higher  $2^+$  states. For JUN45 this is also completely dominated by the state at 2.47 MeV. Thus, this state at 2.47 MeV has the characteristics of the collective mixed-symmetry  $2^+$  state. With the jj44b Hamiltonian the mixed-symmetry configuration is pushed up and fragmented. The largest fragment is at 2.69 MeV.

As noted above, the best experimental candidate for the mixed-symmetry state is at 2766.7 keV with  $B(E2) = 0.33(6)$  W.u. to the ground state and  $B(M1) = 0.24(3) \mu_N^2$  to the first  $2^+$  state. For JUN45, the state at 2.47 MeV with  $B(E2) = 0.74$  W.u. and  $B(M1) = 0.50 \mu_N^2$ , and for jj44b the state at 2.69 MeV with  $B(E2) = 0.13$  W.u. and  $B(M1) = 0.22 \mu_N^2$  can be compared with the mixed-symmetry state. For this isovector state, the result with the jj44b Hamiltonian gives better agreement with experiment. The JUN45 results are worse, probably only because it is 300 keV lower in energy than experiment. Overall, this comparison between experiment and theory presents a beautiful understanding of a mixed-symmetry state in this mass region.

## VI. CONCLUSION

Low-lying, low-spin levels of  $^{76}\text{Ge}$  were investigated extensively with the  $(n, n'\gamma)$  reaction and their properties were characterized. Evidence for a number of previously suggested levels was not found, and their existence is refuted. The revised level scheme and transition strengths for  $^{76}\text{Ge}$  is well

reproduced by large-scale shell model calculations, which provide an excellent description of the structural properties of this nucleus. For the first time, the mixed-symmetry state has been identified and it is supported by microscopic calculations in the shell model. The establishment of the comprehensive level scheme up to near 3 MeV and the observed agreement with shell model calculations shown in this paper provide confidence in the use of the jj44b and JUN45 Hamiltonians for the valence space calculation of the neutrinoless double- $\beta$  decay of  $^{76}\text{Ge}$  [29,30].

## ACKNOWLEDGMENTS

We sincerely thank H. E. Baber for his many contributions to these experiments. This material is based upon work supported by the U.S. National Science Foundation under Grant Nos. PHY-1606890 and PHY-1404442.

## APPENDIX: MODEL SPACES USED IN SHELL MODEL CALCULATIONS

In the NUSHELLX Hamiltonian library [15], the names of some model spaces for heavy nuclei are labeled by the number of orbitals that are between the standard magic numbers;  $k = 4$  ( $0f_{5/2}, 1p_{3/2}, 1p_{1/2}, 0g_{9/2}$ ) for 28–50;  $k = 5$  ( $0g_{5/2}, 1d_{5/2}, 1d_{3/2}, 2s_{1/2}, 0h_{11/2}$ ) for 50–82;  $k = 6$  ( $0h_{9/2}, 1f_{7/2}, 1f_{5/2}, 2p_{3/2}, 2p_{1/2}, 0i_{13/2}$ ) for 82–126; etc. The model space names in proton-neutron formalism where isospin is not necessarily conserved are labeled  $jjk_p k_n pn$ . For example, the model space called  $jj45pn$  is for protons in the group of four above and neutrons in the group of five above. The model space in isospin formalism where total isospin is an explicit quantum number is labeled by  $jjk_p k_n$  (without the  $pn$  on the end). For the calculations in this paper we use the  $jj44$  model space.

Historically, the first  $jj44x$  type of Hamiltonian for this model space is called  $jj44pna$  in the NUSHELLX library for the  $jj44pn$  model space [31]. This Hamiltonian contains one set of two-body matrix elements (TBME) with  $T = 1$  for neutrons that are constrained to reproduce the binding energies and excitation energies for the nickel isotopes ( $Z = 28$ ) with  $N = 33$ –44, and another set of TBME with  $T = 1$  for protons that are constrained to reproduce the binding energies and excitation energies for isotones with  $N = 50$  and  $Z = 32$ –50. The  $jj44pna$  Hamiltonian does not contain proton-neutron TBME and cannot be used away from  $Z = 28$  or  $N = 50$ . For  $jj44pna$  the neutron and proton TBME are different. As a consequence of this, the  $8^+$  seniority isomers obtained in  $^{94}\text{Ru}$  and  $^{96}\text{Pd}$  are not present in the analogous nuclei  $^{72,74}\text{Ni}$  due to a crossing of some states dominated by seniority two and four [31].

For this paper we use the Hamiltonians called  $jj44b$  and JUN45 for the  $jj44$  model space. Both of these contain an assumed mass dependence of  $(A/58)^{-0.3}$ . The TBME for  $jj44b$  are based on those obtained with the renormalized Bonn-C potential. The single-valued decomposition (SVD) method was used to constrain 30 linear combinations of the 133 TBME to 77 binding energies and 470 excitation energies in nuclei with  $Z = 28$ –30 ( $N = 28$ –50), and  $N = 48$ –50

( $Z = 28$ – $50$ ). For a given  $Z$ , the binding energies are corrected by an overall shift obtained from the Coulomb part of a Skyrme energy-density functional calculation. The rms deviation between the theoretical and experimental energies was about 240 keV. These data do not include  $^{76}\text{Ge}$ . When the  $jj44b$  Hamiltonian is used in the proton-neutron model space  $jj44pn$  it is called  $jj44bpn$ ; the results with  $jj44b$  and  $jj44bpn$  are the same. Starting in 2007, the  $jj44b$  Hamiltonian has been used for comparison to data in many publications [where it is sometimes called  $jj4b$  and sometimes cited as B. A. Brown and A. F. Lisetskiy (private communication)] [29,32–41].

The  $T = 1$  TBME for  $jj44b$  are approximately an average of those for protons and neutrons in the the  $jj44pna$  Hamiltonian. When the  $jj44b$  Hamiltonian is applied to

$Z = 28$  or  $N = 50$ , it does work as well as the  $jj44pna$  Hamiltonian. Starting with  $jj44b$ , another Hamiltonian called  $jj44c$  was obtained by leaving out energy data above  $Z = 38$ . This is a better Hamiltonian to use for  $Z = 28$ – $30$ . The  $jj44c$  results for  $^{76}\text{Ge}$  are similar to those for  $jj44b$ .

A method similar to that used to obtain the  $jj44b$  Hamiltonian was used by Honma *et al.* to obtain the JUN45 Hamiltonian [26]. For the JUN45 Hamiltonian, 45 SVD linear combinations were determined by a fit to about 69 binding energies and 330 excitation energies for nuclei in the range  $N = 30$ – $32$  and  $Z = 46$ – $50$ , as shown in Fig. 1 of Ref. [26]. The rms deviation was 185 keV. These data included the ground state and first three excited states in  $^{76}\text{Ge}$ .

- 
- [1] F. T. Avignone, S. R. Elliott, and J. Engel, *Rev. Mod. Phys.* **80**, 481 (2008).
- [2] K. Heyde and J. L. Wood, *Rev. Mod. Phys.* **83**, 1467 (2011).
- [3] A. D. Ayangeakaa, R. V. F. Janssens, C. Y. Wu, J. M. Allmond, J. L. Wood, S. Zhu, M. Albers, S. Almaraz-Calderon, B. Bucher, M. P. Carpenter, C. J. Chiara, D. Cline, H. L. Crawford, H. M. David, J. Harker, A. B. Hayes, C. R. Hoffman, B. P. Kay, K. Kolos, A. Korichi, T. Lauritsen, A. O. Macchiavelli, A. Richard, D. Seweryniak, and A. Wiens, *Phys. Rev. Lett.* **B 754**, 254 (2016).
- [4] A. Gottardo, D. Verney, C. Delafosse, F. Ibrahim, B. Roussi re, C. Sotty, S. Roccia, C. Andreou, C. Costache, M.-C. Delattre, I. Deloncle, A. Etill , S. Franchoo, C. Gaulard, J. Guillot, M. Lebois, M. MacCormick, N. Marginean, R. Marginean, I. Matea, C. Mihai, I. Mitu, L. Olivier, C. Portail, L. Qi, L. Stan, D. Testov, J. Wilson, and D. T. Yordanov, *Phys. Rev. Lett.* **116**, 182501 (2016).
- [5] Y. Toh, C. J. Chiara, E. A. McCutchan, W. B. Walters, R. V. F. Janssens, M. P. Carpenter, S. Zhu, R. Broda, B. Fornal, B. P. Kay, F. G. Kondev, W. Kr las, T. Lauritsen, C. J. Lister, T. Pawlat, D. Seweryniak, I. Stefanescu, N. J. Stone, J. Wrzesiński, K. Higashiyama, and N. Yoshinaga, *Phys. Rev. C* **87**, 041304(R) (2013).
- [6] A. S. Davydov and G. F. Filippov, *Nucl. Phys.* **8**, 237 (1958).
- [7] T. Nikšić, P. Marević, and D. Vretenar, *Phys. Rev. C* **89**, 044325 (2014).
- [8] L. Wilets and M. Jean, *Phys. Rev.* **102**, 788 (1956).
- [9] D. C. Camp and B. P. Foster, *Nucl. Phys. A* **177**, 401 (1971).
- [10] B. Ramstein, R. Tamisier, L. H. Rosier, P. Avignon, and J. P. Delaroche, *Nucl. Phys. A* **411**, 231 (1983).
- [11] B. Sch rmmann, D. Rychel, B. van Kr chten, J. Speer, and C. A. Wiedner, *Nucl. Phys. A* **475**, 361 (1987).
- [12] G. A. Dostemesova, D. K. Kaipov, and Yu. G. Kosyak, *Izv. Akad. Nauk SSSR, Ser. Fiz.* **51**, 1928 (1987) [*Bull. Acad. Sci. USSR, Phys. Ser. (English translation)* **51**, 48 (1987)].
- [13] S. Mordechai, H. T. Fortune, R. Middleton, and G. Stephans, *Phys. Rev. C* **18**, 2498 (1978).
- [14] R. Lecomte, M. Irshad, S. Landsberger, G. Kajrys, P. Paradis, and S. Monaro, *Phys. Rev. C* **22**, 2420 (1980).
- [15] B. A. Brown and W. D. M. Rae, *Nucl. Data Sheets* **120**, 115 (2014).
- [16] P. E. Garrett, N. Warr, and S. W. Yates, *J. Res. Natl. Inst. Stand. Technol.* **105**, 141 (2000).
- [17] A. O. Hansen and J. L. McKibben, *Phys. Rev.* **72**, 673 (1947).
- [18] H. Tagziria and D. J. Thomas, *Nucl. Instrum. Methods* **452**, 470 (2000).
- [19] J. Marion and F. Young, *Nuclear Reaction Analysis: Graphs and Tables* (North Holland Publishing, Amsterdam, 1968).
- [20] E. Sheldon and V. C. Rogers, *Comput. Phys. Commun.* **6**, 99 (1973); P. A. Moldaur, *Phys. Rev. C* **14**, 764 (1976).
- [21] T. Belgya, G. Moln r, and S. W. Yates, *Nucl. Phys. A* **607**, 43 (1996).
- [22] K. B. Winterbon, *Nucl. Phys. A* **246**, 293 (1975).
- [23] B. Singh, *Nucl. Data Sheets* **74**, 63 (1995).
- [24] B. A. Brown and B. H. Wildenthal, *Phys. Rev. C* **21**, 2107(R) (1980).
- [25] N. Pietralla, P. von Brentano, and A. F. Lisetskiy, *Prog. Part. Nucl. Phys.* **60**, 225 (2008).
- [26] M. Honma, T. Otsuka, T. Mizusaki, and M. Hjorth-Jensen, *Phys. Rev. C* **80**, 064323 (2009).
- [27] B. A. Brown (private communication).
- [28] B. P. Crider, E. E. Peters, J. M. Allmond, M. T. McEllistrem, F. M. Prados-Est vez, T. J. Ross, J. R. Vanhoy, and S. W. Yates, *Phys. Rev. C* **92**, 034310 (2015).
- [29] B. A. Brown, D. L. Fang, and M. Horoi, *Phys. Rev. C* **92**, 041301(R) (2015).
- [30] R. A. Senkov and M. Horoi, *Phys. Rev. C* **93**, 044334 (2016).
- [31] A. F. Lisetskiy, B. A. Brown, M. Horoi, and H. Grawe, *Phys. Rev. C* **70**, 044314 (2004).
- [32] D. Verney *et al.*, *Phys. Rev. C* **76**, 054312 (2007).
- [33] K. T. Flanagan *et al.*, *Phys. Rev. C* **82**, 041302(R) (2010).
- [34] A. Gade *et al.*, *Phys. Rev. C* **81**, 064326 (2010).
- [35] B. Cheal, *Phys. Rev. Lett.* **104**, 252502 (2010).
- [36] P. Vingerhoets *et al.*, *Phys. Rev. C* **82**, 064311 (2010).
- [37] A. D. Becerril *et al.*, *Phys. Rev. C* **84**, 041303(R) (2011).
- [38] S. J. Q. Robinson, L. Zamick, and Y. Y. Sharon, *Phys. Rev. C* **83**, 027302 (2011).
- [39] D. Verney *et al.*, *Phys. Rev. C* **87**, 054307 (2013).
- [40] A. C. Dombos *et al.*, *Phys. Rev. C* **93**, 064317 (2016).
- [41] F. Recchia *et al.*, *Phys. Rev. C* **94**, 054324 (2016).